High Cycle Fatigue Analysis in the presence of Autofrettage Compressive Residual Stress

Volodymyr Okorokov [*], Donald MacKenzie[*], Yevgen Gorash [*], Marta Morgantini [*], Ralph van Rijswick[**] and Tugrul Comlekci[***]

[*] University of Strathclyde, 99 George St, Glasgow, G1 1RD, the UK
[**]Weir Minerals, Venlo, 5928 PH
[***] University of the West of Scotland, High Street, Paisley, PA1 2BE, UK

Abstract: An experimental and numerical investigation of the effect of residual compressive stress on the high cycle fatigue life of notched low carbon steel test specimens is presented. Experimentally determined cyclic stress strain curves for S355 low carbon steel are utilized in a Finite Element Analysis plasticity modelling framework incorporating a new cyclic plasticity material model representative of cyclic hardening and softening, cyclic mean stress relaxation and ratcheting behaviors. Fatigue test results are presented for standard tensile fatigue test specimens and novel double notch specimens. Double notch specimens are tested with and without compressive residual stress prior-induced through tensile overload. It is shown that cyclic plasticity phenomena have a significant influence on the induced residual stress distribution and also on material behavior when fatigue tested in the high cycle regime. It is observed that higher initial compressive residual stresses magnitude does not necessarily lead to a longer fatigue life. Finite Element Analysis using the new cyclic plasticity material model shows this behavior is due to combined residual stress redistribution under fatigue test cyclic loading and cyclic hardening effects. A fatigue life methodology based on the stress-life approach augmented by a critical distance method is proposed and shown to give good agreement with experimental results for test specimens with no induced residual stress. The results obtained for specimens with induced residual stress are more conservative but the degree of conservatism is significantly lower than that in the conventional stress life approach. The proposed methodology is therefore suitable for analysis and design assessment of components with pre-service induced compressive residual stress, such as autofrettaged pressure components.

Keywords: Compressive residual stress, Autofrettage, Re-autofrettage, Cyclic plasticity, High cycle fatigue, Theory of critical distance

Nomenclature:

A - material constant for plasticity model

B - material constant for plasticity model

b - material constant for SN curve fitting

L - critical distance parameter

N_f - cycles to failure

n_{ij} - unit direction tensor of plastic flow

O_{ij} - back stress shift tensor

p - accumulated plastic strain

$\dot{p}$ - accumulated plastic strain rate

$\overline{p}$ - previously accumulated plastic strain

$\dot{\overline{p}}$ - previously accumulated plastic strain rate

q - plastic strain amplitude

$\overline{q}$ - previously accumulated plastic strain amplitude

$\dot{\overline{q}}$ - previously accumulated plastic strain amplitude rate

X_{ij} - back stress tensor

γ - material constant for the Walker equation

ΔK_{th} - fatigue crack propagation threshold

ε^e - equivalent elastic strain

ε^p - equivalent plastic strain

ε_{ij}^p - plastic strain tensor

$\dot{\varepsilon}_{ij}^p$ - plastic strain rate tensor

σ_a - uniaxial stress amplitude

σ_{ar} - equivalent completely reversed stress amplitude

σ_m - uniaxial mean stress

$\sigma_{\max}$ - uniaxial maximum stress

$\sigma_{\min}$ - uniaxial minimum stress

σ_f - fatigue limit at a given R ratio

σ'_f - material constant for SN curve fitting

σ_{eq} - equivalent von Mises stress

σ_{eq}^a - equivalent stress amplitude

σ_{eq}^m - equivalent mean stress

$\sigma_{11}^a, \sigma_{22}^a, \sigma_{33}^a$ - normal components of the stress amplitude tensor

$\sigma_{11}^m, \sigma_{22}^m, \sigma_{33}^m$ - normal components of the mean stress

$\tau_{12}^a, \tau_{23}^a, \tau_{31}^a$ - shear components of the stress amplitude tensor

τ - time delay

1. Introduction

Autofrettage is an established method for increasing the fatigue life of components subject to cyclic or repeated pressure loading. The basis of the method is to induce limited plastic strain in the component through initial application of a relatively high autofrettage pressure. When the component is depressurized, a self-equilibrating residual stress system is established, with compressive residual stress in regions experiencing plastic deformation during loading. When the component is subsequently pressurized under operating conditions, the mean stress in these regions is lower than that in similar non-autofrettage components, leading to extended fatigue life.

Experimental and theoretical investigations of autofrettage commonly focus on two topics: calculation of the induced residual stress distribution and methods to predict the fatigue life in the presence of residual stress. The accuracy of the residual stresses calculation is determined by the nature of the elastic-plastic analysis employed and the elastic-plastic material data available. Analytical approaches based on the deformation theory of plasticity have been proposed from early [1-4] through to more recent [5-9] studies. This type of analysis is limited to proportional loading, relatively simple component geometry and single applications of autofrettage pressure. More complex problems are generally analyzed using numerical methods, in particular the Finite Element Method, FEM. The accuracy of the FEM approach is dependent, *inter alia*, on the plasticity model employed. Commercial FEM programs usually include several different plasticity models. The most widely used models in general elastic-plastic analysis are based on relatively simple kinematic and isotropic hardening rules. These models can represent several different features of elastic-plastic deformation but they do not, in general, fully represent the behavior of a material subject to plastic cycling. Application of cyclic loads in excess of the initial yield strength of the material can induce cyclic plasticity phenomena such as mean stress relaxation, ratcheting, cyclic softening and hardening and changing elastic properties during plastic strain accumulation. These responses are not captured by a linear kinematic hardening plasticity material model: a cyclic plasticity material model is required.

A standard autofrettage process consists of a single “overload” of the pressure component. However, multiple application of overload pressure can enhance the established residual stress field and extend fatigue life. Proposed procedures include multiple autofrettage with intermediate and post-autofrettage thermal treatment [10, 11] and double autofrettage with application of lower overload pressure in the second autofrettage cycle [12]. In the former procedure, the enhanced residual stress is attributed to microstructural changes occurring during the thermal treatment processes which leads to negation of the Bauschinger effect. In the latter procedure, which does not incorporate thermal treatment, the enhanced response is attributed to changes of cyclic hardening properties from the first autofrettage overload.

Several material models addressing the specific requirements of cyclic plasticity behavior have been proposed in the literature [13-16]. These models utilize different flow rules for kinematic and isotropic hardening and show good agreement with material tests for prediction of ratcheting rate and calculation of a stabilized stress strain state under cyclic softening or hardening. In the re-autofrettage process, the material experiences only a few reloading cycles and the main challenge is to establish an accurate model of the stress-strain behavior at the transition between the initial monotonic stress-strain curve and subsequent cyclic stress-strain curves. Models based on a modified Armstrong-Fredrick nonlinear kinematic rule with Chaboche back stress decomposition have been shown to give accurate prediction of compressive residual stress in this type of application [17, 18]. However, these models require a large number of back stress decompositions and the complicated theoretical framework can pose problems in engineering application.

Experimental studies have shown that fatigue strength can be greatly increased through application of autofrettage processes. Application of a low temperature autofrettage process was found to result in a greater than 40% increase in fatigue limit[19]. Other autofrettage studies have reported fatigue strength increase in excess of 60% [20-26]. However, the optimum autofrettage conditions for extended fatigue life have not been fully established. It is usually expected that optimum autofrettage condition is achieved when the maximum compressive residual stresses magnitude is induced. Residual stress relaxation due to thermal and plasticity effects is known to occur following mechanical treatment processes such as shot peening, deep rolling and low plasticity burnishing [27] but this effect has not been studied in depth for autofrettage. The conventional approach to determining the fatigue life of autofrettage components usually assumes wholly elastic material behavior under operating conditions. Any changes that may occur in the autofrettage residual stress distribution due to cyclic operating loads is not usually considered. However, it is known that limited plastic strain may occur in some materials when cyclically loaded below the fatigue limit [28]. Such cyclic plastic deformation may induce some redistribution of the residual stress field.

In high cycle fatigue analysis, it is convenient to divide the total fatigue life into two stages: crack initiation and crack propagation. The fatigue life of most engineering components is dominated by the crack initiation stage. However, when the component has been subjected to autofrettage, the induced compressive residual stress can retard fatigue crack growth and in some circumstances fully arrest crack propagation. A study of plasticity induced fatigue crack closure for autofrettaged intersecting holes[29] found that autofrettaged samples demonstrating infinite fatigue life actually cracked after a finite number of cycles. These initial cracks were arrested during propagation due to a barrier of compressive residual stresses induced by autofrettage. Similar crack arrest effects were also observed in studies of diesel-engine injection tubes[30, 31]. Accurate determination of crack propagation time in the presence of these phenomena requires application of fracture mechanics methods. To define the total fatigue life, the crack initiation time must also be determined. Fatigue crack initiation in metals is associated with the nucleation and propagation of microstructurally and mechanically short cracks. Standard Linear Elastic Fracture Mechanics approaches are not appropriate in analysis of short cracks. Advanced fracture mechanics methods [32-34] can be employed but these are not always suitable for prediction of the fatigue life of complex engineering components. The theory of critical distances [35-38] provides an alternative approach to the problem. The critical distances method has been shown to give accurate fatigue strength predictions for a range of elastic components with different forms of stress concentration features and has been extended to assessment of autofrettaged components by incorporating a critical distance parameter in the stress-life fatigue methodology [39].

This paper presents the results of a combined experimental and numerical investigation of the fatigue behavior of S355 low carbon steel in the presence of an induced residual stress field. The specific motivation for the investigation was to better understand the effect of autofrettage and multiple-autofrettage on the fatigue life of industrial pump components. However, the methodology adopted in the experimental and analysis elements of the study are general and relevant to a wide range of industry applications. The experimental study is based around a pre-stressed, double-notch tensile test specimen with induced residual stress. The specimen is designed to give a residual stress field similar in form and magnitude to that commonly found in pressure components with stress raising features, such as cross-bores, after application of autofrettage. Similar notch or stress raising features are found in many other engineering applications. In the present study, the double notch specimen provides a simple, representative model of the behavior of pressure components without recourse to complex cyclic pressure testing. The simplified arrangement allows investigation of the effect of different overloading conditions corresponding to different autofrettage pressures on high cycle fatigue strength, enabling optimum autofrettage conditions to be determined and validated experimentally.

The elastic-plastic deformation of the specimen during initial overload and subsequent cyclic operating conditions is investigated through a Finite Element Analysis, FEA, framework incorporating a new material model formulated for cyclic plasticity applications [40]. The cyclic plasticity model provides an accurate representation of the material cyclic stress-strain response, including cyclic hardening, softening, mean stress relaxation and ratcheting effects, through of a small number of material constants. This enables accurate evaluation of the development of residual stress during the initial overload procedure, including multiple overloads, and any subsequent plastic deformation processes that may occur during operating (or fatigue) loading cycles. The proposed FEA framework, coupled with theory of critical distance evaluation of fatigue crack initiation, provides a coherent methodology for determining the fatigue life of pre-stressed components.

2. Plasticity Material Properties and Material Model

An autofrettage residual stress field arises from limited plastic deformation of a component induced during pressure loading: either by a single application or multiple applications of the autofrettage pressure. FEM determination of the induced residual stress field requires a plasticity material model that can fully represent the cyclic plastic behavior of the material and associated material property data.

The material considered here is a general purpose low carbon steel, S355. Monotonic and cyclic stress strain curves for the material were obtained by tension-compression testing of rectangular test specimens, as shown in Fig. 1, on a 250 kN servo-hydraulic testing machine under both strain and force control. Strain was measured using a 10 mm gauge length extensometer. The cyclic plasticity loading programs were chosen to quantify the phenomena of cyclic hardening and softening, cyclic mean stress relaxation and ratcheting. Both low and high strain rate tests were performed: with low strain rates representative of autofrettage loading conditions and high strain rate loading representative of cycling under operating (fatigue) loading conditions.

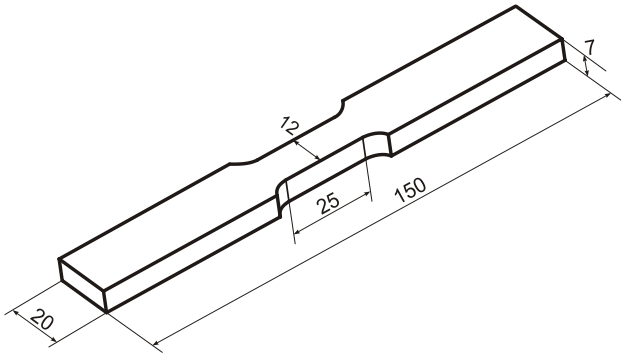

Fig. 1 – Tensile-compression sample geometry

2.1 Cyclic plasticity constitutive modelling

The cyclic plasticity material model used in the investigation is a recent formulation [40] that incorporates all cyclic plasticity phenomena expected under cyclic loading. The model incorporates a novel set of internal variables which represent strain range dependence effects and transition from the initial monotonic stress-strain curve to subsequent cyclic loading curves. These are incorporated into the constitutive model through introduction of a Dirac delta function $\delta(Z)$ with argument:

$$Z = \frac{1}{2}\left[p - p' + \mathbb{S}\left(\varepsilon^{p} - \varepsilon^{p'} \right) \right] \tag{1}$$

where ε^p and p are equivalent and accumulated plastic strain at time t respectively, $\varepsilon^{p'}$ and p' are equivalent and accumulated plastic strain at previous time $(t-\tau)$ and $\mathbb{S}$ is a sign operator, which changes sign with a simultaneous sign change in $\frac{d\sigma_{eq}}{dp}$, $\frac{d\varepsilon^p}{dp}$ and $\frac{d\varepsilon^e}{dp}$. Equivalent plastic strain ε^p is defined as:

$$\varepsilon^p = \sqrt{\frac{2}{3}\varepsilon_{ij}^p \varepsilon_{ij}^p} \tag{2}$$

and accumulated plastic strain rate $\dot{p}$ is defined as:

$$\dot{p} = \sqrt{\frac{2}{3}\dot{\varepsilon}_{ij}^p \dot{\varepsilon}_{ij}^p} \tag{3}$$

The Dirac function thus returns an instant change of internal variables when a change in flow direction occurs at the start of a new load step. At other times, it returns a zero value and the variables remain unchanged. The variables are therefore constants during the current load step and change value only at the beginning of the next step. For example, the instant change of the plastic strain amplitude and previously accumulated plastic strain at time *t* can be introduced by:

$$\dot{\bar{q}} = [p - \bar{p}' - 2\bar{q}']\delta(Z)\dot{p} \tag{4}$$

$$\dot{\bar{p}} = [p - \bar{p}']\delta(Z)\dot{p} \tag{5}$$

where $\bar{q}'$ and $\bar{p}'$ are the plastic strain amplitude and previously accumulated plastic strain respectively defined at previous time $(t-\tau)$:

$$\bar{q}' = \bar{q}(t-\tau) \tag{6}$$

$$\bar{p}' = \bar{p}(t-\tau) \tag{7}$$

An accurate representation of the stress-strain curve is achieved by introducing a new expression of the kinematic hardening rule:

$$\dot{X}_{ij} = AB\exp\left(-\frac{1}{B}\frac{X_{ij} - O_{ij}}{n_{ij}}\right)\dot{\varepsilon}_{ij}^p \tag{8}$$

where X_{ij} is the back stress tensor, O_{ij} is the back stress shift tensor, A and B are plasticity model material constants and n_{ij} is the unit direction tensor of plastic flow. This approach accurately describes the stress-strain curve in terms of two material constants. Similar accuracy using an Armstrong-Fredrick type of kinematic hardening rule requires 8 Chaboche back stress decompositions (16 material constants). The new model can predict the ratcheting rate or stresses at a stabilized state after cyclic hardening or softening under cyclic loading and can accurately describe the stress-strain curve shape at any loading condition. Increased accuracy in cyclic hardening and softening is achieved by introducing strain range dependence into constants of the kinematic hardening rules A and B. This is of specific relevance when modelling autofrettage and re-

autofrettage processes and compressive residual stress redistribution during the initial cycles of operating load.

Stress-strain paths calculated by the new model are compared with experimental load-unload stress-strain data for S460N steel [17] and alternative cyclic plasticity models of Jiang *et al* [16] and Döring *et al* [17] in Fig. 2. The load-unload paths predicted by the present model exhibit close agreement with the experimental data other than at a small region at the initiation of the plateau. High accuracy is due to the particular form of back stress shift tensor O_{ij}, which is formulated by a combination of Dirac delta functions and Heaviside step functions and uses the same material constants for all curves in the deformation process as the back stress tensor. In comparison, the Jiang model[16] is in good agreement for unloading but does not fully capture the initial monotonic curve. The Döring model[17] gives a better representation of the monotonic curve but is less accurate than the other models for unloading, particularly in the small plastic strain region. The new model is intended for general application and is not limited to analysis of steels. The general form of equation (8) is valid for a wide range of materials, with the evolution rule for the back stress shift tensor O_{ij} developed for each specific material. The cyclic plasticity response predicted for D16 aluminium alloy is compared with experimental data[41] in Fig. 3. This is a challenging simulation, the initial monotonic curve has almost linear plastic hardening while all subsequent curves are significantly non-linear. The present model is able to accurately simulate this material behavior.

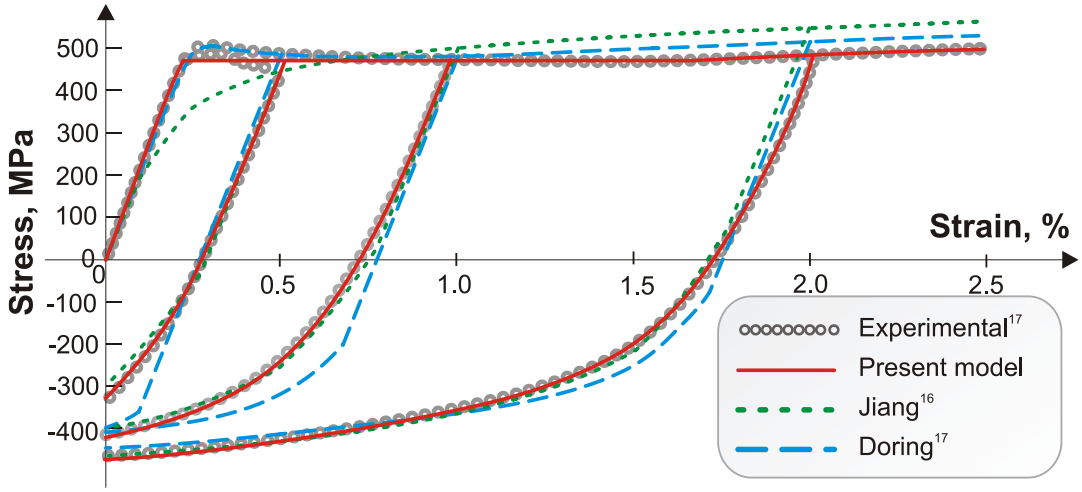

Fig. 2 – Loading-unloading stress-strain responses for S460N from [17] and simulation by different plasticity models

Experimental cyclic plasticity test results for the S355 steel of the present study are shown in Fig. 4 for two cycles of loading at low and high strain rates. These demonstrate strain rate dependence in the plasticity response, with the higher strain rate giving a higher yield stress and different strain hardening effect. As most engineering high cycle fatigue loading conditions have loading frequencies above 0.1 Hz, this rate dependency is relevant when modelling plasticity phenomena which occur during the fatigue lifetime. The stress-strain paths calculated by the new plasticity material model show that the kinematic hardening rule accurately describes the shape of the stress-strain curves.

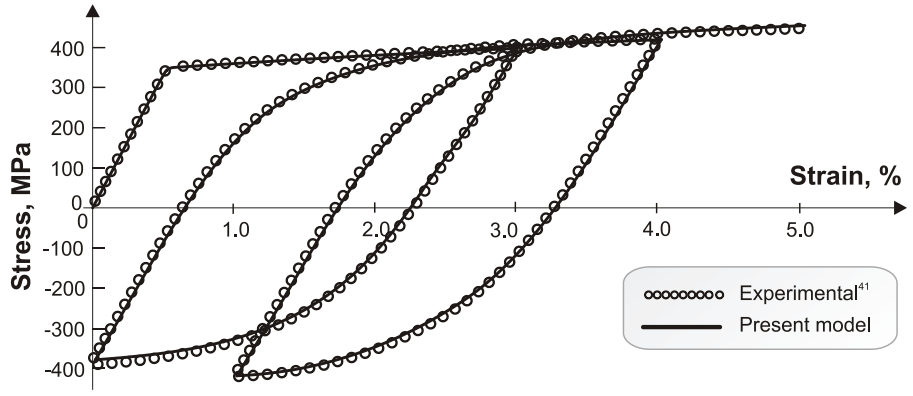

Fig. 3 – Cyclic stress-strain response of D16 aluminum alloy with numerical simulations

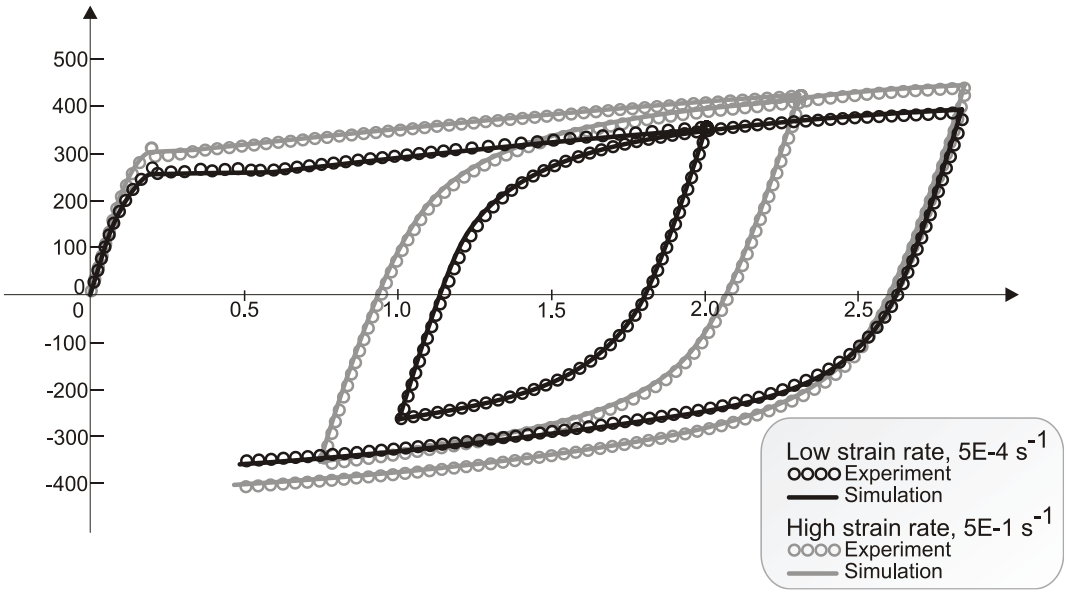

Fig. 4 – Stress-strain curves of S355 at two strain rates of loading

2.2 Mixed cyclic hardening and softening

Most engineering metals exhibit cyclic hardening or cyclic softening. These phenomena suggest that values of peak stresses in stable hysteresis loops depend on the strain range of cyclic loading. To examine the effect of cyclic hardening or softening of the S355 steel, increasing level tests [42], in which the strain magnitude is increased after stress stabilization, were performed. The results obtained are compared with the monotonic stress-strain curve in Fig. 5. This shows the material has mixed cyclic hardening and softening. For strain amplitude up to 0.3%, the material cyclically softens and the material deviates from linear elastic behavior at stresses below the monotonic yield stress (initiation of the plateau in the monotonic curve). The set of internal variables used in the plasticity model is able to simulate the effect of cyclic softening when cyclic loading occurs below the initial monotonic yield stress. For strain amplitude greater than 0.3%, the material shows significant cyclic hardening. Cyclic hardening and softening effects are usually neglected when modelling autofrettage but Fig. 5 suggests that these may have a significant effect on the calculated residual stress, particularly for multiple autofrettage. The strain range dependence incorporated in the proposed cyclic plasticity framework exhibits good agreement with experimental observations.

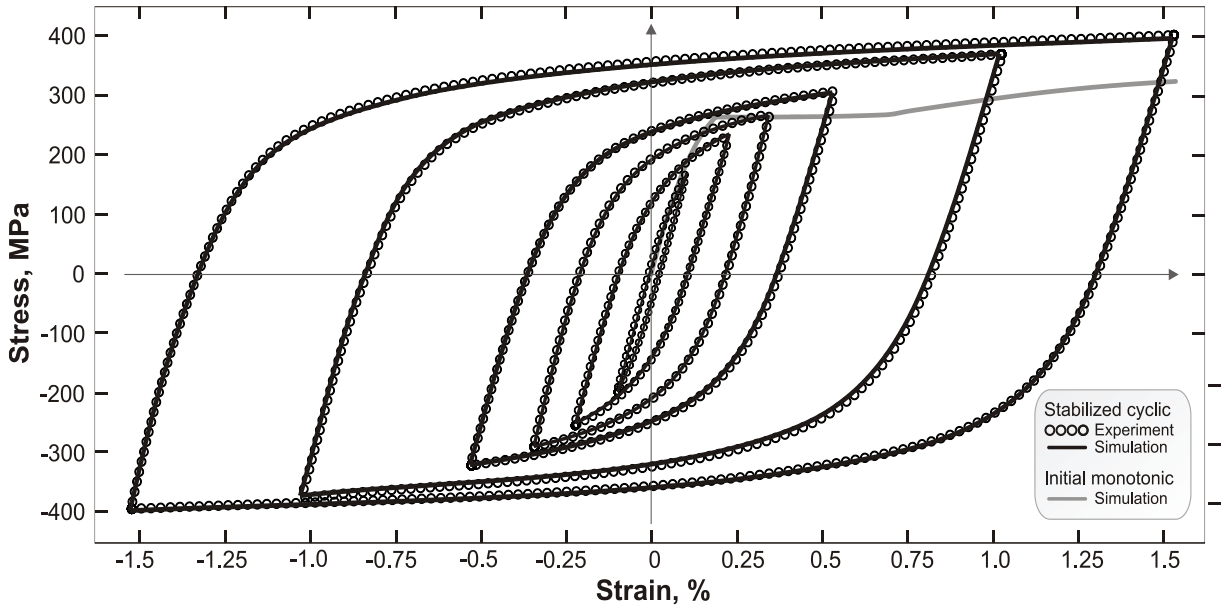

Fig. 5 – S355 steel increasing level test results

2.3 Cyclic mean stress relaxation and ratcheting

Cyclic mean stress relaxation occurs under fixed strain amplitude cyclic loading with non-zero mean strain. The stress-strain response obtained from a mean stress relaxation test of S355 is shown in Fig. 6. Repeated application of load with fixed strain amplitude reduces the mean stress of loading and increases the compressive part. In multiple applications of autofrettage, this behavior, in conjunction with cyclic hardening, can lead to increased magnitude of compressive residual stress. Ratcheting occurs under fixed force amplitude cyclic loading with non-zero mean force. The response of the S355 material tested under this form of loading is shown in Fig. 7. The paths calculated by the proposed plasticity model are seen to be closely representative of the ratcheting rate and cyclic stress-strain curves. Under multiaxial loading, mean stress relaxation and ratcheting may occur together. Both of these are represented in the new plasticity model. During multiple application of autofrettage loads, these effects can enhance the compressive residual stresses but may also lead to increased mean stress under operating conditions.

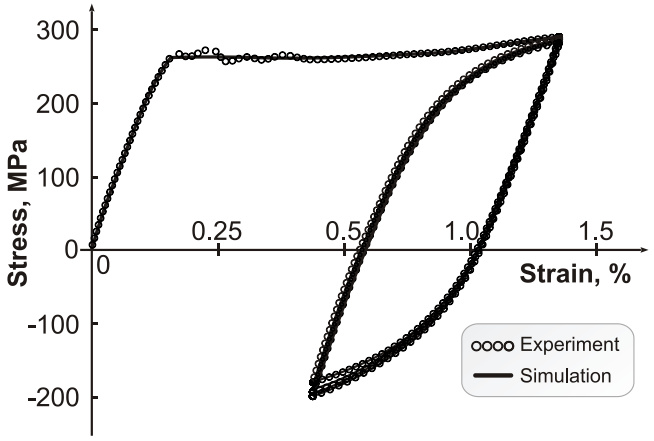

Fig. 6 – S355 steel cyclic mean stress relaxation

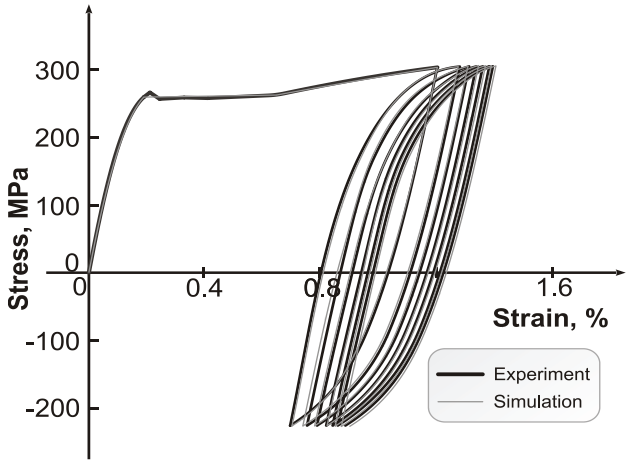

Fig. 7 – S355 steel ratcheting

3. Uniaxial fatigue testing

Uniaxial fatigue tests were conducted for cylindrical low carbon steel specimens, as shown in Fig. 8, on a 150 kN servo-hydraulic testing machine under the force control at frequency 15 Hz. The load ratios considered were R = 0 and R = -1, where:

$$R = \frac{\sigma_{\min}}{\sigma_{\max}} \tag{9}$$

The fatigue life data obtained are shown in Fig. 9a, with SN curves approximated by Basquin's power law:

$$\sigma_a = \sigma'_f \left(2N_f\right)^b \tag{10}$$

The effect of mean stress on fatigue life is presented in the form of a Haigh diagram in Fig. 9b. Mean stress correction is based on the Walker equation:

$$\sigma_{ar} = \sigma_a \left(\frac{2}{1-R}\right)^{1-\gamma} \tag{11}$$

which has been shown to be representative of the mean stress effect in steels [43]. The constants determined for the fatigue behavior of the uniaxial samples are given in Table 1.

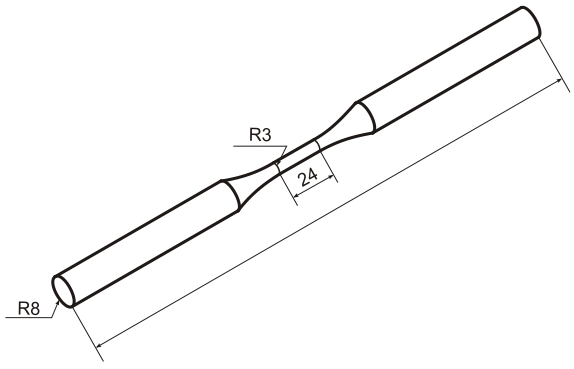

Fig. 8 – Uniaxial fatigue specimen geometry

Table 1 – Fatigue parameters of the uniaxial test

Type of loading	σ_f , MPa	σ'_f	b	ΔK_{th}	γ
R = -1	211	393	-0.04	12	0.73
R = 0	172	430	-0.06	8	

Fig. 9b shows that for loading ratios in the range R > -0.2, the maximum stress is greater than the initial yield stress of the material. This indicates significant plastic strain accumulates during the first fatigue load cycle. The effect of plasticity ratcheting is present for loading below the fatigue limit observed in Fig 9a. Cyclic plasticity phenomena can therefore occur in the high cycle fatigue region of 10^5 – 10^7 cycles and when a uniaxial sample exhibits infinite life. However, Fig. 5 and Fig. 6 show that the loading process stabilizes after finite number of cycles, typically 30 to 50 cycles. Therefore, in this investigation the cyclic plasticity response is modelled for a limited number of cycles to accurately determine the stabilized stress-strain cycle.

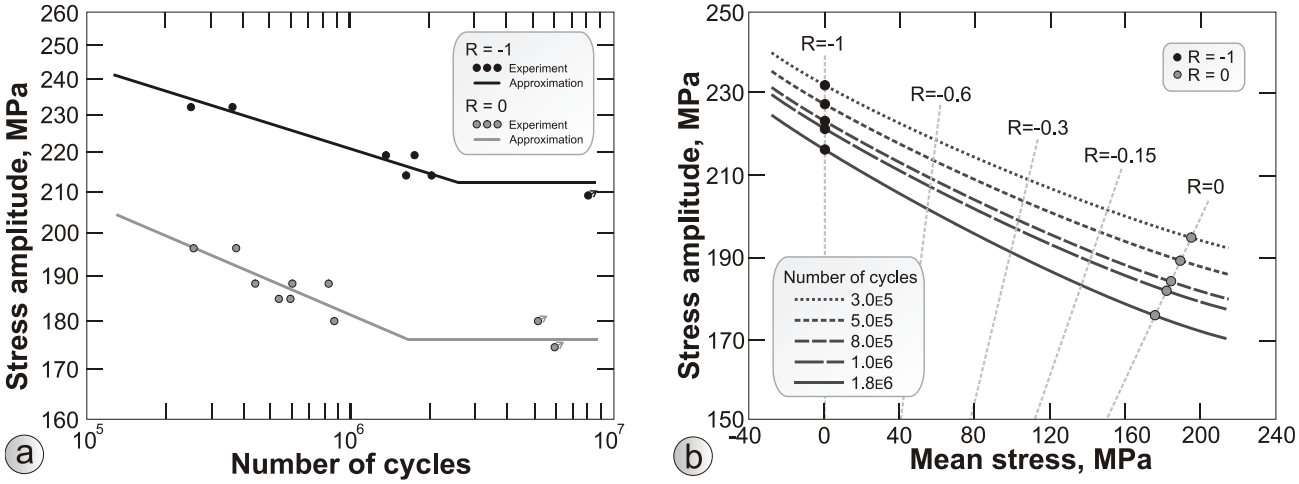

Fig. 9 – Results of uniaxial fatigue testing in terms of a) SN curve and b) Haigh diagram

4. Fatigue life prediction methodology

The proposed test methodology considers the behavior of pre-stressed double notched tensile test specimens with geometry as defined in Fig. 10. Compressive residual stress is induced in the specimen prior to fatigue testing by initially subjecting it to an "autofrettage" tensile force sufficient to cause limited plastic deformation in the notch region. First yield occurs at the four notch intersection regions of the specimen. Plastic deformation spreads from these locations into the specimen by a limited amount, such that the core of the specimen remains elastic. When the axial load is subsequently reduced to zero, a self-equilibrating state of residual stress is established with tensile stress in the elastic core and compressive stress in the regions of plastic deformation.

4.1 Residual stress prediction

Finite Element Analysis, FEA, of the plastic deformation processes was performed using the ANSYS Workbench program[44]. A 3D model of a 1/16 segment of the specimen geometry was created, as shown in Fig. 11, meshed by higher order tetrahedral elements. Symmetry boundary conditions were applied at the three symmetry planes. The autofrettage force is applied as a remote tensile force at the sample ends. Elastic-

plastic analysis was performed using two material models: the new plasticity model of Section 2.1 implemented as an ANSYS Workbench User Programmable Feature (UPF) and the standard ANSYS Chaboche nonlinear kinematic hardening model with the best fit to the experimental data. Geometric nonlinear effects were included when total strain values exceeded 3%.

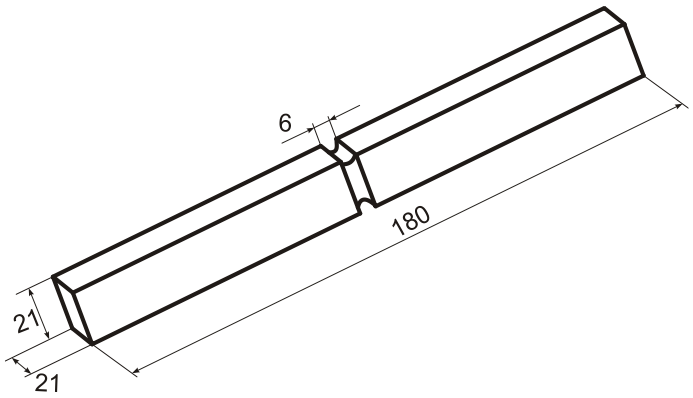

Fig. 10 – Sample geometry for fatigue testing with the autofrettage effect

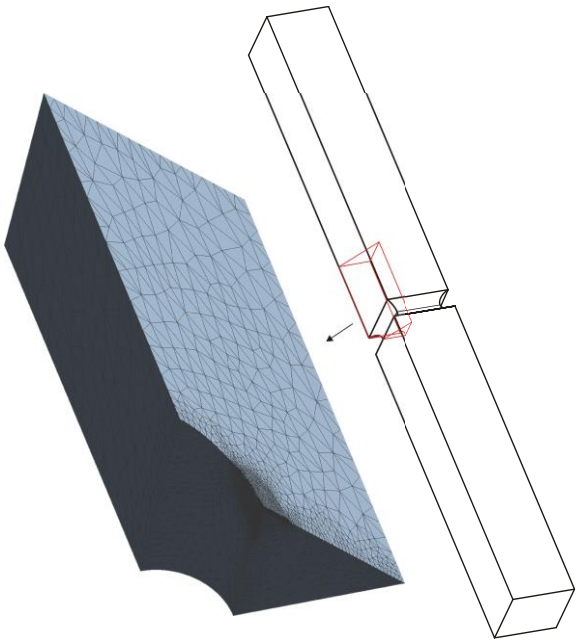

Fig. 11 – 1/16th symmetric specimen FE mesh

Contour plots of the residual stress fields for tensile loading to 65 kN then unloading to zero evaluated by the new plasticity model and the Chaboche model are shown in Fig. 12a and Fig. 12b respectively. The two material models give significantly different magnitudes and distributions of calculated compressive residual stresses. In this application, the Chaboche model does not represent the form of the material stress-strain relationship during loading and unloading as closely as the new model, as shown in the inset stress-strain plots of Fig. 12.

The magnitude of notch root compressive residual stresses calculated using the new plasticity model is dependent on the value of autofrettage force and the number of times it is applied, as shown in Fig. 13a for single and multiple (10) applications. The residual stress magnitude increased with increasing force for both cases. For forces below 45 kN, the residual stress induced by multiple overload is slightly less than that for a single application, due to cyclic softening effects at small plastic strain amplitude. At higher overloading forces, multiple autofrettage induces higher compressive residual stress. The accumulation of total strain with increasing autofrettage overload for single and multiple (10) applications is shown in Fig. 13b. Comparison with Fig. 13a shows that increasing the total strain above 5% gives only a 3% increase in compressive residual stress at the notch root. From a practical point of view, it is recommended that autofrettage overload should satisfy a limiting value of accumulated strain, as excessive overload can create structural damage to the component.

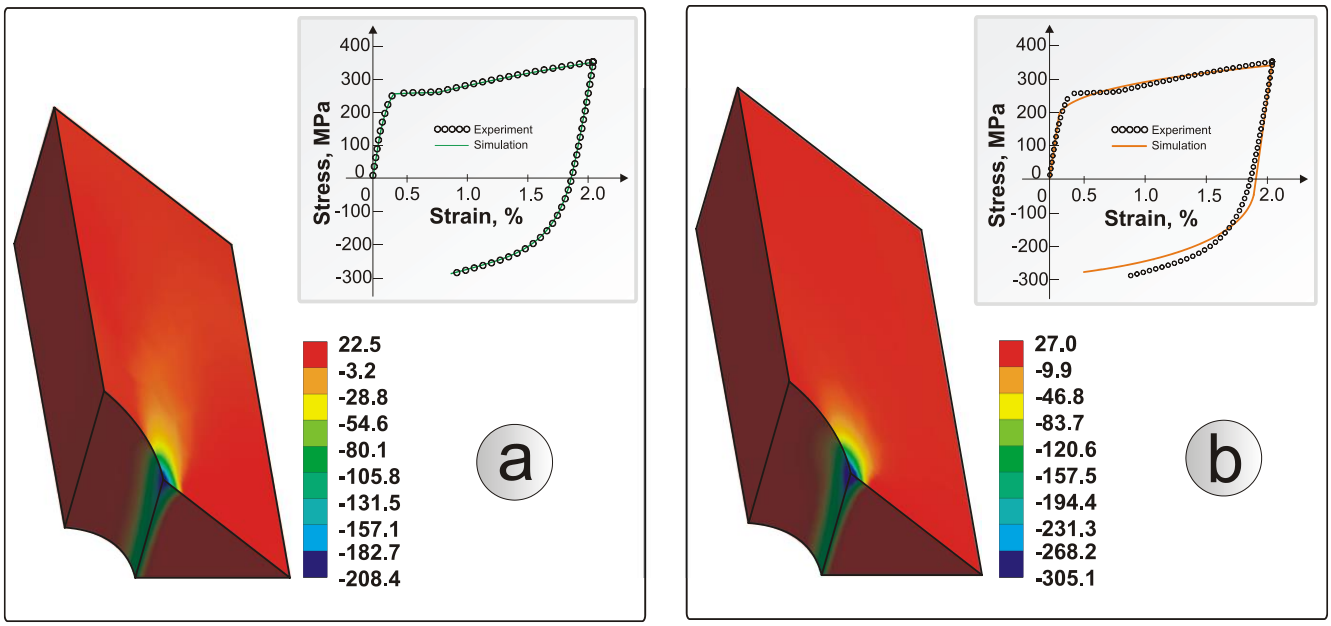

Fig. 12 – Distribution of the compressive residual stress (minimum principal stress) calculated using a) the new plasticity model and b) the ANSYS Chaboche nonlinear kinematic hardening model

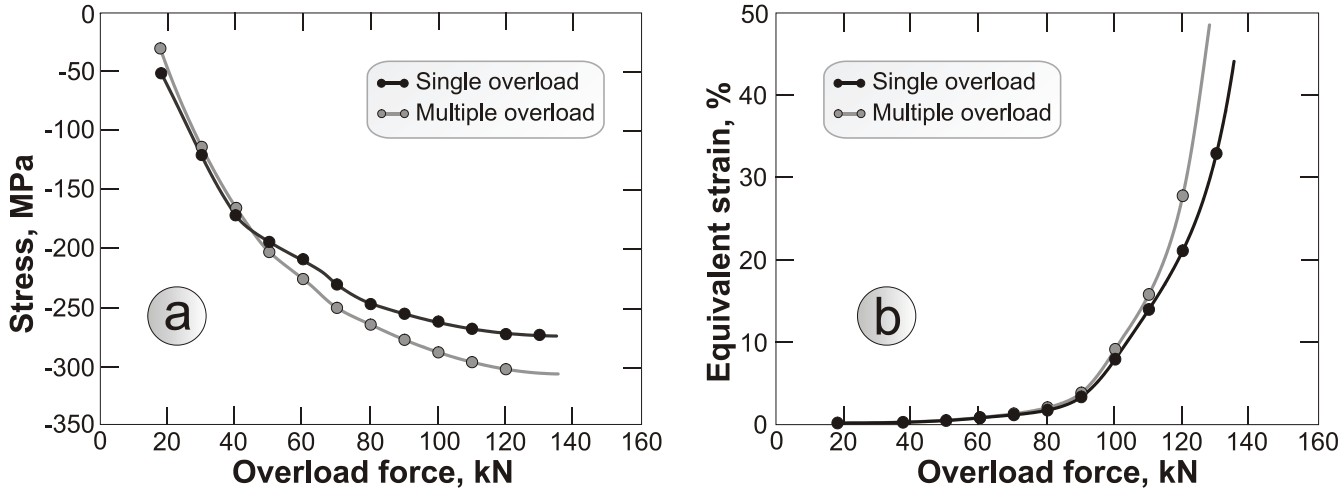

Fig. 13 – Dependence of the a) compressive residual stress and b) equivalent total strain on the overload force

4.2 Fatigue tests

Fatigue testing was performed for specimens with no induced residual stress and for individual specimens with different degrees of pre-stress: single overload of 55kN, 75kN, 92kN and 140kN and 10 applications of overload of 75kN. The greatest compressive residual stress was calculated for specimens subject to 10 cycles of 75kN of overload by FEA. In single preload specimens, the greatest compressive residual stress was calculated in specimens subject to 92kN, then 75kN, 55kN and 140kN respectively. Two special cases of overload were also considered: a single application of 140kN, which is close to the fracture strength of the specimen, and a single application of compressive load -87kN, inducing tensile residual stress in the notched region of the specimen. The specimens were subject to fatigue test under alternating axial force with loading ratio of R = 0.

The test results summarized in Fig. 14 indicate that the fatigue life of pre-stressed specimens is not solely determined by the magnitude of residual stress induced during preloading alone but is also dependent on cyclic plastic strain accumulation during the fatigue test. The longest fatigue life observed in all tests was for specimens with a single preload of 75kN. These specimen did not have the highest calculated compressive residual stress, which occurred for multiple application of the 75kN force. The latter specimens exhibited shorter fatigue life than single 75kN pre-load specimens at 22kN, 23kN and 25kN alternating force. At 25kN alternating test force, the fatigue life of the multiple preload specimens was less than that of specimens with no induced compressive residual stress and at 22kN the fatigue life was similar. The ratcheting test results of Fig. 7 show that significant plastic strain accumulation can occur in S355 steel in the high-cycle fatigue range considered here. This behavior can lead to changes in compressive residual stress in specimens (including establishment of residual stress in non-preloaded specimens) as cyclic plasticity stabilization occurs during initial cycles of the fatigue test.

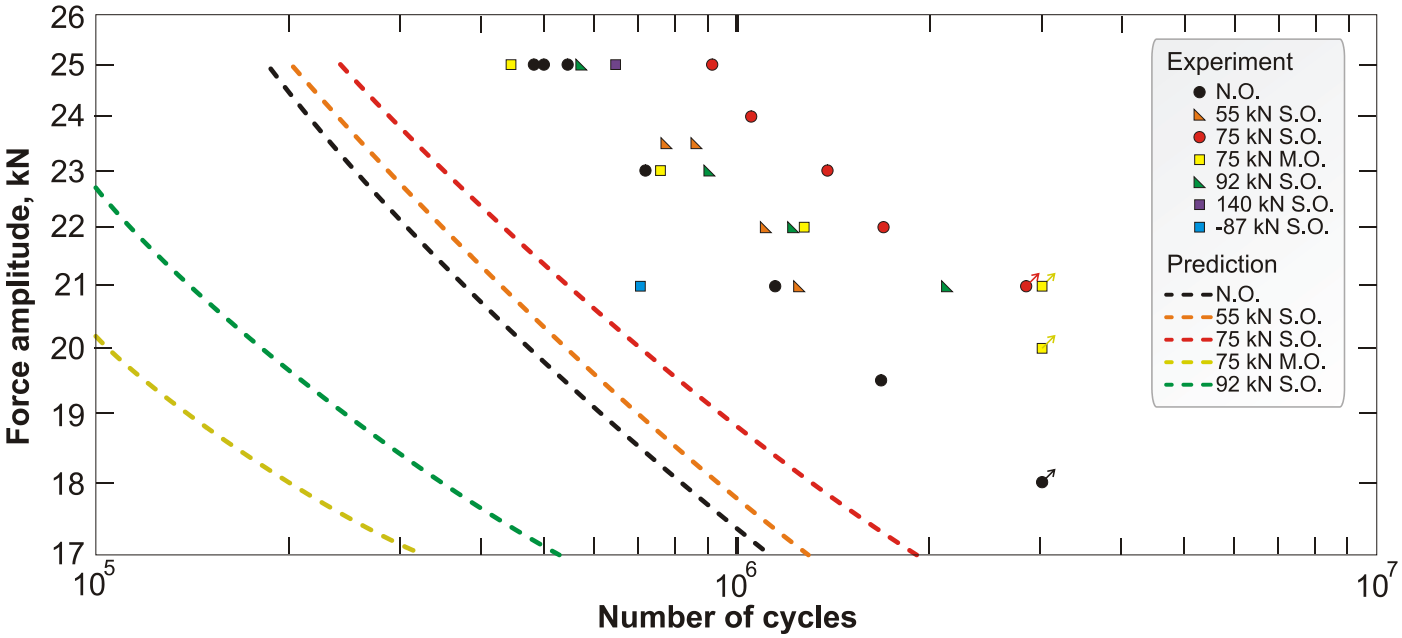

Fig. 14 – Results of fatigue testing of notched samples together with standard stress life predictions, where N.O. – no overload, S.O. – single overload and M.O. – multiple overload

The specimen subject to an initial tensile force of 140 kN (close to the fracture strength of the specimen) was tested under an alternating force of 25kN. The initial preload of this specimen may cause significant material damage in highly loaded regions due to nucleation of voids and micro-discontinuities. This would be expected to significantly reduce the fatigue life. However, the test result indicates that in practice a small improvement in fatigue life occurred. This may be attributed to the differing nature of plastic damage accumulation during monotonic or low cycle fatigue loading and the damage accumulation process of high cycle fatigue. The high compressive residual stresses induced by overloading can block fatigue crack propagation initiated from damage accumulation due to large plastic strains. The specimen subject to an initial compressive force of -87kN was tested under an alternating force of 21kN. This exhibited a shorter fatigue life than a specimen with no pre-stressing, attributed to the tensile residual stress in the specimen.

4.3 Calculation of fatigue life

In stress life fatigue analysis, the stress cycle at a point in a body is defined between two specific load states by the mean stress and stress amplitude. In 3D analysis, nominal scalar values of mean stress and stress amplitude are determined by application of a multiaxial criterion, usually corresponding to a multiaxial yield criterion such as Maximum Principal Stress, Tresca or von Mises. The Tresca criterion may be incorporated in a critical plane analysis framework approach[45]. The stress life procedure applied here is based on the von Mises criterion, assuming proportionality of effective mean stress and hydrostatic pressure[46]. The equivalent stress amplitude and mean stress are defined as:

$$\sigma_{eq}^{a} = \frac{1}{\sqrt{2}}\sqrt{\left(\sigma_{11}^{a}-\sigma_{22}^{a}\right)^{2}+\left(\sigma_{22}^{a}-\sigma_{33}^{a}\right)^{2}+\left(\sigma_{33}^{a}-\sigma_{11}^{a}\right)^{2}+6\left(\tau_{12}^{a\,2}+\tau_{23}^{a\,2}+\tau_{31}^{a\,2}\right)} \tag{12}$$

$$\sigma_{eq}^{m} = \sigma_{11}^{m}+\sigma_{22}^{m}+\sigma_{33}^{m} \tag{13}$$

The procedure is illustrated for a specimen initially subject to 75 kN multiple preload and tested under 21kN cyclic load. Fig. 15 shows the calculated distribution of equivalent stress amplitude, the corresponding equivalent mean stress and stress ratio. Redistribution of initial compressive residual stress due to cyclic plasticity effects is simulated by application of 50 cycles of test force amplitude. The maximum equivalent stress amplitude occurs at the notch root. Although the remote force applied to the ends of the sample has load ratio R = 0, the stress ratio in the notched region varies significantly due to the compressive residual stresses induced prior to cyclic loading, ranging from R = -2.11 to R = 0.8.

The fatigue life of each specimen is evaluated by comparing the calculated maximum equivalent stress amplitude at the notch root with the experimental uniaxial SN curves and Haigh diagram of Fig. 9b. Fatigue life curves calculated using this approach shown in Fig. 14 are seen to significantly underestimate the observed experimental values. For example, the maximum notch root equivalent alternating stress of the 75 kN multiple overload specimen tested under 21 kN force amplitude was 254 MPa. Comparing this to the uniaxial experimental data gives a fatigue life of around $5\text{x}10^5$ cycles, whereas the tested specimen exhibited run-out at $3\text{x}10^6$.

The underestimation of the fatigue life of components with stress concentration has been previously reported in the literature [35-39, 47]. In the stress based approach, the fatigue life assessment is based on stress at a point. However, a fatigue crack is initiated due to stresses acting on a process volume of material. Consequently, to predict the fatigue life of a component incorporating a stress concentration feature, averaged stresses acting on the process volume should be calculated. A limited number of empirical formulas have been

proposed in the literature to incorporate the stress concentration effect and make predictions in better agreement with experimental results. These approaches are usually empirical, dependent on material and component geometry and do not have a theoretical basis. An alternative approach to the problem is adopted in the theory of critical distance. This theory generalizes fatigue strength for different geometries and stress concentration features by introducing a unique parameter which can be calibrated from fatigue tests of notched specimens and, in some cases, can be directly derived from fracture mechanics. The unique parameter is a critical distance over which the average stresses are calculated. The aim is to represent the process volume of material which actually influences the fatigue strength. There are several options for the critical distance approach in which stresses are averaged over either a line, area or volume. In the simplest option, the critical distance is determined with the use of a fracture mechanics approach as [35]:

$$L = \frac{1}{\pi}\left(\frac{\Delta K_{th}}{2\sigma_f}\right)^2 \tag{14}$$

The prediction of the fatigue limit of a component with a stress concentration is then made according to [35]:

$$\sigma_{eq}^{a}(L/2) = \sigma_f \tag{15}$$

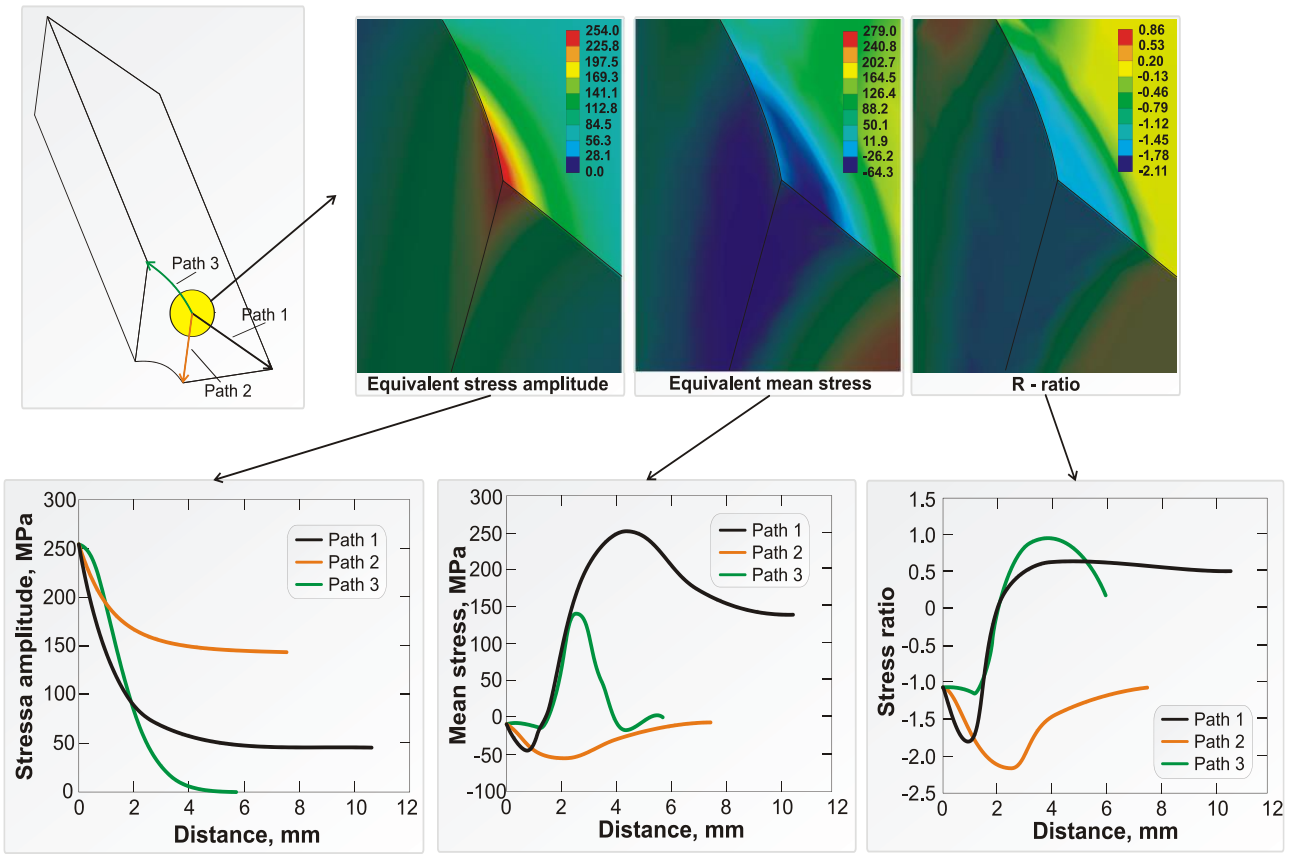

Fig. 15 – Distribution of equivalent stress amplitude, equivalent mean stress and stress ratio at the notch area of the sample

A development of the method for prediction of finite fatigue life is presented in[47], where the critical distance parameter is derived as a function of the number of cycles. This approach has shown accurate prediction of fatigue life for members incorporating stress concentration features in several different applications. The method is attractive in that reasonable accuracy is achieved from FEM calculations with the

use of only a few parameters. However, the method is not directly applicable in the presence of a residual stress field, as parameters are derived or calibrated assuming a constant R-ratio corresponding to the applied load ratio. In the case of cyclic loading with induced residual stress, the stress R-ratio is not constant, as illustrated in Fig. 15. This problem may be overcome by a modified critical distance method in which an iterative procedure is applied to determine an average value of R-ratio in a specific region[39]. Here, the calculated stresses are averaged over Path 1 of Fig. 15. Fatigue life predictions using this approach for four different pre-load cases (including no preload) are presented in Fig. 16. These show good agreement with experimental results for non-overloaded samples, Fig. 16a. However, the predictions for the overloaded samples in Fig. 16b, 16c and 16d are more conservative, but significantly less conservative than conventional stress life prediction, as given in Figure 14. This difference is attributed to retardation of fatigue crack growth due to compressive residual stresses at the notch area (in the case of the overloaded samples, the long crack propagation stage can take up to 20% of the total fatigue life). Fig. 15 shows that the mean stress starts to decrease achieving its minimum at around 1 mm away from the notch root. A crack initiating at the notch root under high stress amplitude propagates into a field of decreasing stress amplitude and lower mean stress, where it propagates less rapidly. More accurate fatigue life prediction can be achieved by incorporating further analysis of crack propagation.

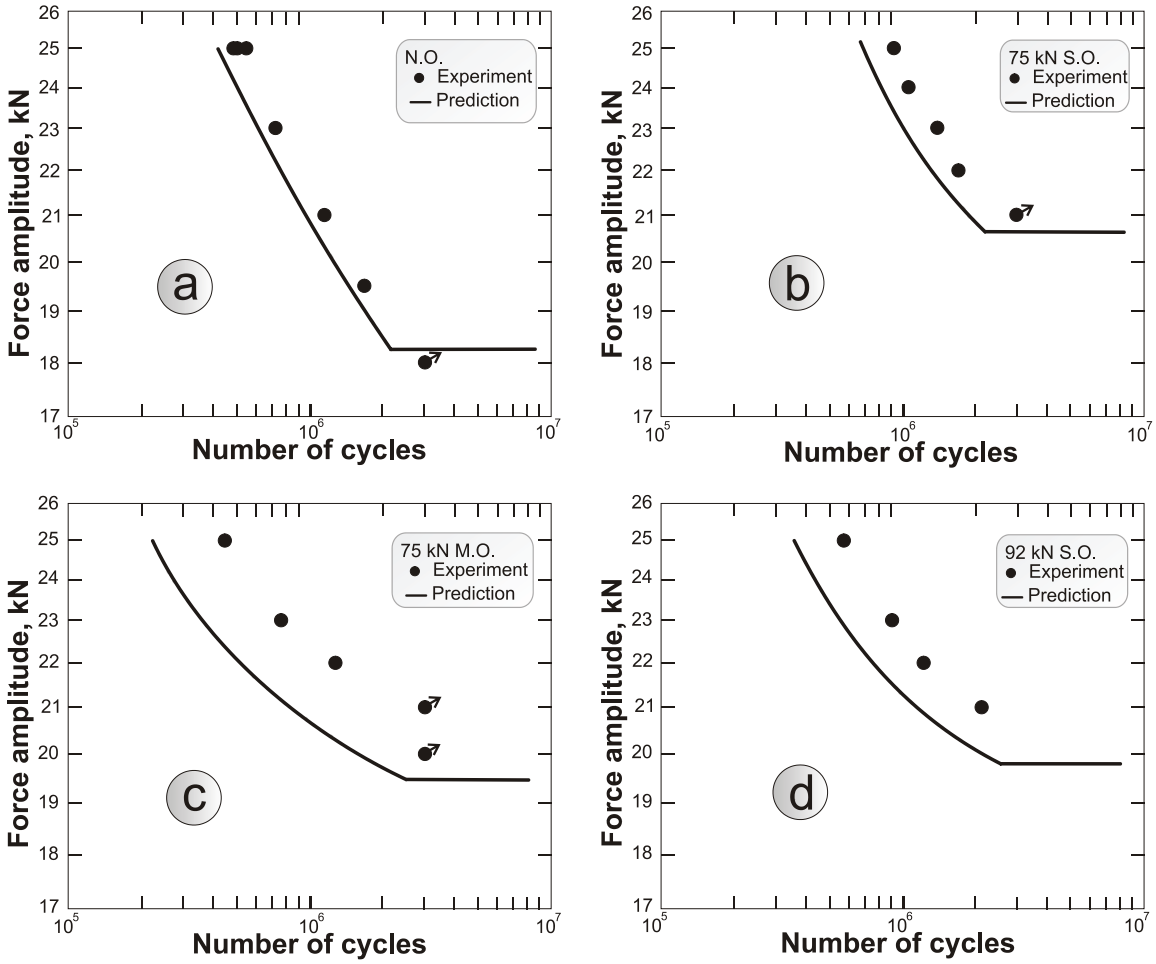

Fig. 16 – Experimental results of fatigue testing of notched sample with predictions by modified critical distance method for the cases of a) no autofrettage overload, b) 75 kN of single autofrettage overload, c) 75 kN of multiple re-autofrettage overload and d) 92 kN of single autofrettage overload; N.O. = No Overload, S.O. = Single Overload and M.O. = Multiple Overload

4.4 Plasticity effects

The influence of plasticity effects on high cycle fatigue behavior during cyclic loading is considered for two autofrettage conditions: single and multiple autofrettage overload of 75 kN. A single load application induces a calculated compressive residual stress of -244 MPa of at the notch root. Application of 10 cycles of 75 kN results in a notch root compressive stress of -267 MPa. The fatigue test results of Fig. 14 show that the single application of preload leads to a longer fatigue life than the multiple application. This behavior can be understood by considering the calculated equivalent stress amplitude and mean stress obtained during application of the working load cycle. Table 2 and Table 3 show the calculated equivalent stress amplitude and mean stress averaged over the critical distance parameter for both autofrettage conditions at 4 applied cyclic load levels. In all cases, the multiple re-autofrettage overload leads to lower mean stress but increases the stress amplitude. This leads to a shorter fatigue life for the multiple overloaded specimens compared to the single overloaded specimens, despite the lower initial compressive residual stress in the notch area induced by multiple autofrettage.

Table 2 –Numerical calculation results for 75 kN single autofrettage overload

Alternating force, kN	25	23	22	21
Equivalent stress amplitude (averaged over the critical distance), MPa	223.2	227.7	220.1	219.8
Equivalent mean stress(averaged over the critical distance)	-1.7	-12.5	-18.3	-24.7
R – ratio (averaged over the critical distance)	-1.01	-1.12	-1.18	-1.25
Predicted number of cycles to failure, N	7.1E5	1.0E6	1.4E6	1.8E6
Critical distance, mm	0.5	0.37	0.33	0.31

Table 3 – Results of numerical calculation for 75 kN multiple re-autofrettage overload

Alternating force, kN	25	23	22	21
Equivalent stress amplitude (averaged over the critical distance), MPa	240.3	242.4	234.0	229.9
Equivalent mean stress(averaged over the critical distance)	-21.2	-27.5	-37.4	-42.6
R – ratio (averaged over the critical distance)	-1.19	-1.26	-1.38	-1.48
Predicted number of cycles to failure, N	2.1E5	3.8E5	5.5E5	8.9E5
Critical distance, mm	0.62	0.55	0.49	0.45

The conventional understanding that higher autofrettage compressive residual stress will lead to longer fatigue life is valid only if the structural response to the working fatigue loading is purely elastic. In that case, the applied load amplitude gives rise to the same stress amplitude irrespective of the value of residual stresses. However, the present investigation shows that the assumption of purely elastic loading may not lead to accurate prediction of fatigue life. In the case of the S355 low carbon steel considered here, the material demonstrates cyclic hardening with accumulation of plastic strain within the high cycle fatigue range. Application of a higher overload force and initial working load cycles both harden the material stress-strain response and result in a higher stress amplitude for the same value of loading amplitude. Fig. 17 shows the calculated stress-strain relationship during fatigue loading cycles of amplitude 25 kN. Two preload conditions are shown: no overload and single overload of 92 kN. In both cases, after the initial overload and shakedown effects, fatigue loading leads to a stabilized cycle. In the overloading case, the stabilized cycle has a compressive mean stress of -8 MPa and stress amplitude of 163 MPa. In the no overload case, the mean stress is 47 MPa and stress amplitude is 144 MPa. Although the overloaded sample has a lower stabilized mean

stress, its fatigue life is shorter due to the higher stress amplitude. This is explained by the plasticity influence on the stress amplitude of fatigue working loading condition. Considering these findings, the re-autofrettage process is not beneficial in terms of the fatigue life improvement for this class of carbon steels. However, when fatigue with environmental effects is considered the re-autofrettage process may be the most appropriate case. Fatigue life can be significantly reduced by corrosion effects in low carbon steels, such that the applied loads should be significantly lower than in the case of fatigue in air. In this case, the plastic part of strains can be insignificant and can be neglected. Therefore, the stress amplitudes are not dependent on the plasticity effects, so that the largest field of compressive residual stresses will provide the longest fatigue life in the very high cycle region of 10^8 – 10^9 cycles.

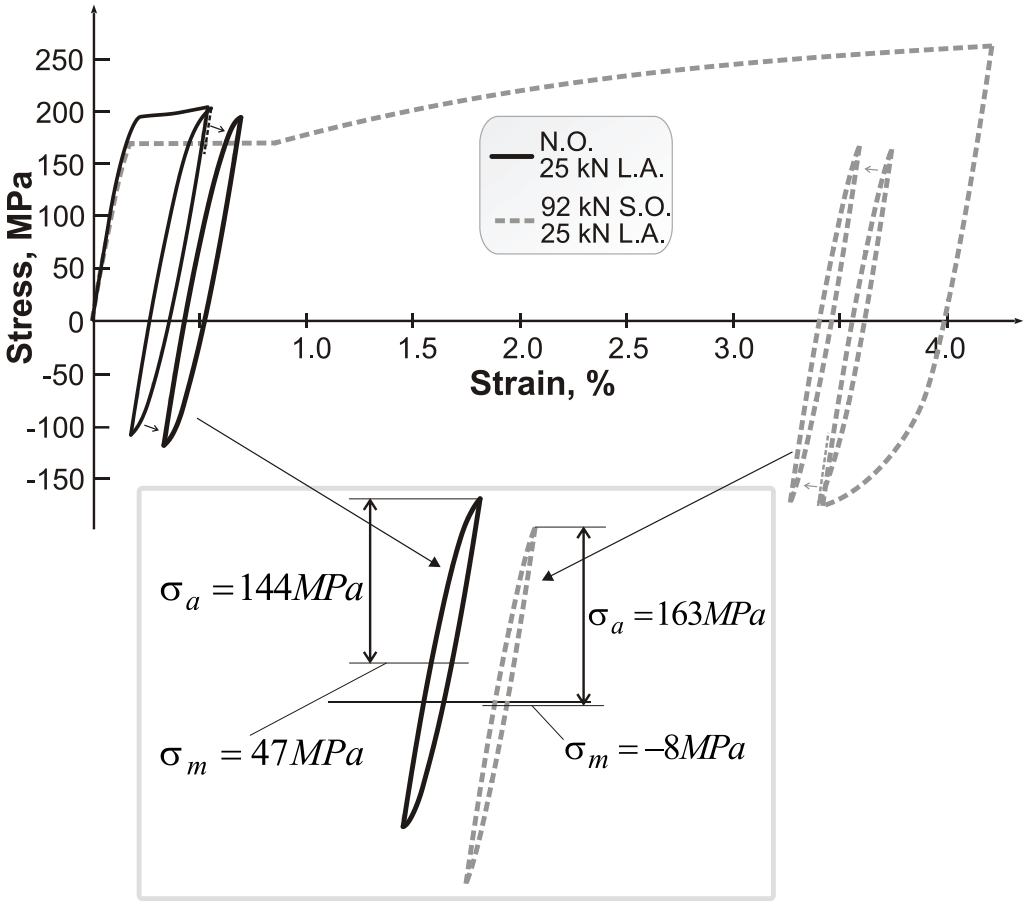

Fig. 17 – Deviatoric axial stress vs. axial plastic strain at the notch root during both the autofrettage process and fatigue cycling, where N.O. = No Overload, S.O. – Single Overload and L.A. = Loading Amplitude

5. Engineering Applications

Stress-life fatigue analysis is widely used in many areas of engineering due to the relative ease of application of the methodology. Design and assessment procedures based on the stress life approach are intentionally conservative however it is known that in certain situations the degree of conservatism can be excessive. Structures and components containing stress raising features are particularly liable to over-conservatism. This is clearly illustrated by comparison of the fatigue test results and stress life predictions for the double notch specimens used in the present study, shown in Fig. 14. Use of more advanced techniques based on fracture mechanics concepts can provide more accurate determination of the total fatigue life of

cyclically loaded components but these usually require more specialist knowledge, non-standard material models and access to high performance computing facilities. The methodology proposed here bridges the complexity and associated degree of conservatism of these approaches.

The proposed methodology has two main features: use of an advanced cyclic plasticity material model to fully represent any cyclic plasticity behavior occurring under cyclic loading and application of the critical distance theory to determine fatigue crack initiation. The motivation for the present study was to better understand the role of autofrettage and other residual stress methods in the fatigue life of pump components in the mining and minerals industries. However, the findings are relevant to wider engineering application, for structures and components with and without induced residual stress. The methodology is suited to engineering design calculations in an industry environment. In the present application, the cyclic plasticity model was implemented as a User Programmable Feature (UPF) and applied in FEA in the same manner as a standard ANSYS material model. The critical distance methodology used to determine the crack initiation and short crack propagation stages of fatigue life are also amenable to industry use in that only a small number of material parameters are required. The critical distance method is limited in that it cannot represent propagation of long cracks. This limitation is not significant for most fatigue life applications, where the total fatigue life is dominated by the crack initiation stage. However, the presence of compressive residual stress due to autofrettage and similar processes can greatly extend the propagation stage. In such applications, the critical distance approach gives conservative values for total fatigue life. However, the degree of conservatism may be significantly less than conventional stress-life fatigue analysis and is suitable for design and structural integrity assessment applications.

The fatigue test results show that multiple application of overload can increase the magnitude of compressive residual stress induced in an autofrettaged component. However, the cyclic hardening characteristics of the material can influence its response during fatigue loading cycles, leading to higher stress amplitude. In this way, the fatigue life of a multiple autofrettaged component may be less than that of a similar single autofrettage component or even a component with no autofrettage, as seen in the fatigue test results for S355 low carbon steel in Fig. 14. However, this behavior is not necessarily general to all materials and re-autofrettage may be beneficial for high strength materials exhibiting cyclic softening.

6. Conclusions

This results of the experimental and FEM investigation of the fatigue life of double notched S355 low carbon steel specimens with and without induced compressive residual stress show that the behavior of pre-stressed components under cyclic loading is complex and dependent on the material response, component geometry and the nature and magnitude of loading. The analysis framework adopted incorporates a new cyclic plasticity material model that can represent cyclic plastic material behavior (cyclic hardening, cyclic softening, mean stress relaxation and ratcheting) in terms of a limited number of material constants. The model provides detailed and accurate evaluation of the formation of the residual stress field in the component and any subsequent plastic deformation processes that occur under operating conditions: i.e. fatigue load cycles in the fatigue test program. The augmented stress-life fatigue methodology proposed incorporates a critical distance parameter representative of notch effects in the presence of residual stress.

FEA of the plastic deformation of the double notch S355 low carbon steel specimens subjected to both single and multiple overload showed that repeated application of the same overload can induce higher magnitude compressive residual stress in the specimen notch region. However, the fatigue tests showed that the subsequent fatigue life of the specimens was not dependent on the magnitude of induced compressive

residual stress alone. In some cases where fatigue failure occurred before 10^6 cycles, multiple overload specimens demonstrated lower fatigue life than similar specimens with no induced compressive stress. This finding is perhaps contrary to general understanding of induced compressive residual stress procedures. The FEA investigation showed that the lower fatigue life is a consequence of the significant cyclic hardening behavior of S355 low carbon steel, which leads to larger stress amplitude occurring in the multiple overload specimens during fatigue cycle loading. This behavior may be typical for low strength materials that cyclically harden and experience plastic strain accumulation during high cycle fatigue loading.

The fatigue test results presented indicate that conventional stress-life fatigue assessment can significantly underestimate the experimentally observed high cycle fatigue life of double notch tensile test specimens. In the methodology proposed here, this conservatism is addressed by introduction of a critical distance parameter in the fatigue life assessment procedure. The methodology is shown to give good agreement with experimental results for the fatigue life of specimens without pre-induced compressive residual stress. However, predictions of the fatigue life for overloaded samples are conservative, although less than conventional stress life analysis. This is a limitation of the critical distance approach, which provides accurate calculation of the crack initiation time but does not account for crack growth retardation in overloaded samples, where the induced compressive residual stress creates a significant barrier to the growth of initiated cracks, resulting in a longer fatigue life than predicted. More accurate prediction could be obtained by adopting a more complex fracture mechanics approach for crack growth calculations but the simpler critical distance method provides a viable methodology for design rule applications, as it provides accurate determination of crack initiation time and is a conservative measure of the total fatigue life.

Acknowledgements

This project has received funding from the European Union's Horizon 2020 research and innovation programme under the Marie Sklodowska-Currie grant agreement No 643159.

References

1. Hill R (1950) *The Mathematical theory of plasticity, by R. Hill*. The Clarendon Press, Oxford.
2. Thomas DGB (1953) The autofrettage of thick tubes with free ends. *Journal of the Mechanics and Physics of Solids*. **1**: 124-133.
3. Rees DWA (1987) A theory of autofrettage with applications to creep and fatigue. *International Journal of Pressure Vessels and Piping*. **30**: 57-76.
4. Parker AP, Farrow JR (1981) Stress intensity factors for multiple radial cracks emanating from the bore of an autofrettaged or thermally stressed, thick cylinder. *Engineering Fracture Mechanics*. **14**: 237-241.
5. Adibi-Asl R, Livieri P (2006) Analytical Approach in Autofrettaged Spherical Pressure Vessels Considering the Bauschinger Effect. *Journal of Pressure Vessel Technology*. **129**: 411-419.
6. Hojjati MH, Hassani A (2007) Theoretical and finite-element modeling of autofrettage process in strain-hardening thick-walled cylinders. *International Journal of Pressure Vessels and Piping*. **84**: 310-319.
7. Haghpanah Jahromi B, Farrahi GH, Maleki M, Nayeb-Hashemi H, Vaziri A (2009) Residual stresses in autofrettaged vessel made of functionally graded material. *Engineering Structures*. **31**: 2930-2935.
8. Wen J-F, Gao X-L, Xuan F-Z, Tu S-T (2017) Autofrettage and shakedown analyses of an internally pressurized thick-walled spherical shell based on two strain gradient plasticity solutions. *Acta Mechanica*. **228**: 89-105.
9. Altenbach H, Lvov G, Naumenko K, Okorokov V (2016) Consideration of damage in the analysis of autofrettage of thick-walled pressure vessels. *Proceedings of the Institution of Mechanical Engineers, Part C: Journal of Mechanical Engineering Science*. **230**: 3585-3593.
10. Parker AP (2004) A Re-Autofrettage Procedure for Mitigation of Bauschinger Effect in Thick Cylinders. *Journal of Pressure Vessel Technology*. **126**: 451-454.

11. Troiano E, Underwood JH, Parker AP, Mossey C (2010) Post-Autofrettage Thermal Treatment and Its Effect on Reyielding of High Strength Pressure Vessel Steels. *Journal of Pressure Vessel Technology*. **132**: 061402-061402-061405.
12. Jahed H, Moghadam BA, Shambooli M (2005) Re-Autofrettage. *Journal of Pressure Vessel Technology*. **128**: 223-226.
13. Lee C-H, Do VNV, Chang K-H (2014) Analysis of uniaxial ratcheting behavior and cyclic mean stress relaxation of a duplex stainless steel. *International Journal of Plasticity*. **62**: 17-33.
14. Xu L, Nie X, Fan J, Tao M, Ding R (2016) Cyclic hardening and softening behavior of the low yield point steel BLY160: Experimental response and constitutive modeling. *International Journal of Plasticity*. **78**: 44-63.
15. Feigenbaum HP, Dugdale J, Dafalias YF, Kourousis KI, Plesek J (2012) Multiaxial ratcheting with advanced kinematic and directional distortional hardening rules. *International Journal of Solids and Structures*. **49**: 3063-3076.
16. Jiang Y, Sehitoglu H (1996) Modeling of Cyclic Ratchetting Plasticity, Part I: Development of Constitutive Relations. *Journal of Applied Mechanics*. **63**: 720-725.
17. Döring R, Hoffmeyer J, Seeger T, Vormwald M (2003) A plasticity model for calculating stress–strain sequences under multiaxial nonproportional cyclic loading. *Computational Materials Science*. **28**: 587-596.
18. Voyiadjis GZ, Hoseini SH, Farrahi GH (2012) A Plasticity Model for Metals With Dependency on All the Stress Invariants. *Journal of Engineering Materials and Technology*. **135**: 011002-011002-011013.
19. Mughrabi H, Donth B, Vetter G (1997) LOW-TEMPERATURE AUTOFRETTAGE: AN IMPROVED TECHNIQUE TO ENHANCE THE FATIGUE RESISTANCE OF THICK-WALLED TUBES AGAINST PULSATING INTERNAL PRESSURE. *Fatigue & Fracture of Engineering Materials & Structures*. **20**: 595-604.
20. Rees DWA (1991) THE FATIGUE LIFE OF THICK-WALLED AUTOFRETTAGED CYLINDERS WITH CLOSED ENDS. *Fatigue & Fracture of Engineering Materials & Structures*. **14**: 51-68.
21. Sellen S, Maas S, Andreas T, Plapper P, Zürbes A, Becker D (2015) Improved design of threaded connections by autofrettage in aluminium compounds for cyclic high pressure loading: design calculations and experimental verification. *Fatigue & Fracture of Engineering Materials & Structures*. **38**: 714-729.
22. Thumser R, Bergmann JW, Herz E, Hertel O, Vormwald M (2008) Variable amplitude fatigue of autofrettaged diesel injection parts. *Materialwissenschaft und Werkstofftechnik*. **39**: 719-725.
23. Pölzl M, Schedelmaier J (2003) Fatigue Strength Curves of Thick Walled Tubes Under Consideration of Autofrettage. 85-90.
24. Lee S-I, Koh S-K (2002) Residual stress effects on the fatigue life of an externally grooved thick-walled pressure vessel. *International Journal of Pressure Vessels and Piping*. **79**: 119-126.
25. Badr E, Sorem J, Tipton S (2000) Evaluation of the Autofrettage Effect on Fatigue Lives of Steel Blocks with Crossbores Using a Statistical and a Strain-Based Method.
26. Underwood JH, Parker AP, Corrigan DJ, Audino MJ (1996) Fatigue Life Measurements and Analysis for Overstrained Tubes With Evacuator Holes. *Journal of Pressure Vessel Technology*. **118**: 424-428.
27. McClung RC (2007) A literature survey on the stability and significance of residual stresses during fatigue. *Fatigue & Fracture of Engineering Materials & Structures*. **30**: 173-205.
28. Boller C, Seeger T (1987) *Materials Data for Cyclic Loading: Low-alloy steels*. Elsevier.
29. Herz E, Hertel O, Vormwald M (2011) Numerical simulation of plasticity induced fatigue crack opening and closure for autofrettaged intersecting holes. *Engineering Fracture Mechanics*. **78**: 559-572.
30. Herz E, Thumser R, Bergmann JW, Vormwald M (2006) Endurance limit of autofrettaged Diesel-engine injection tubes with defects. *Engineering Fracture Mechanics*. **73**: 3-21.
31. Sellen S, Maas S, Andreas T, Plapper P, Zürbes A, Becker D (2016) Design rules for autofrettage of an aluminium valve body. *Fatigue & Fracture of Engineering Materials & Structures*. **39**: 68-78.
32. Hertel O, Vormwald M (2014) Multiaxial fatigue assessment based on a short crack growth concept. *Theoretical and Applied Fracture Mechanics*. **73**: 17-26.
33. Hertel O, Vormwald M (2011) Short-crack-growth-based fatigue assessment of notched components under multiaxial variable amplitude loading. *Engineering Fracture Mechanics*. **78**: 1614-1627.

34. Döring R, Hoffmeyer J, Seeger T, Vormwald M (2006) Short fatigue crack growth under nonproportional multiaxial elastic–plastic strains. *International Journal of Fatigue*. **28**: 972-982.
35. Taylor D (2008) The theory of critical distances. *Engineering Fracture Mechanics*. **75**: 1696-1705.
36. Taylor D, Bologna P, Bel Knani K (2000) Prediction of fatigue failure location on a component using a critical distance method. *International Journal of Fatigue*. **22**: 735-742.
37. Susmel L (2008) The theory of critical distances: a review of its applications in fatigue. *Engineering Fracture Mechanics*. **75**: 1706-1724.
38. Susmel L, Taylor D (2006) A simplified approach to apply the theory of critical distances to notched components under torsional fatigue loading. *International Journal of Fatigue*. **28**: 417-430.
39. Okorokov V, Gorash Y, Morgantini M, MacKenzie D, Rijswick R, Comlekci T (2017) An extension of the theory of critical distance to fatigue life predictions with residual stress effects. *International Journal of Fatigue*. In submission.
40. Okorokov V, Gorash Y, MacKenzie D, Rijswick R, Comlekci T (2017) A Cyclic Plasticity Model with a New Formulation of Nonlinear Kinematic Hardening. *International Journal of Plasticity*. In submission.
41. Okorokov V (2014) Experimental Determination of the Bauschinger Effect and Material Damage *NTU «KhPI» Bulletin: Series «Dynamics and Strength of Machines»*. **58**: 141-153.
42. Nouailhas D, Cailletaud G, Policella H, et al. (1985) On the description of cyclic hardening and initial cold working. *Engineering Fracture Mechanics*. **21**: 887-895.
43. Dowling NE, Calhoun CA, Arcari A (2009) Mean stress effects in stress-life fatigue and the Walker equation. *Fatigue & Fracture of Engineering Materials & Structures*. **32**: 163-179.
44. (2016) ANSYS Workbench 18.0 edn, Canonsburg, PA.
45. Li H, Johnston R, Mackenzie D (2010) Effect of Autofrettage in the Thick-Walled Cylinder With a Radial Cross-Bore. *Journal of Pressure Vessel Technology*. **132**: 011205-011205-011205.
46. Dowling NE (1993) *Mechanical Behavior of Materials: Engineering Methods for Deformation, Fracture, and Fatigue*. Prentice Hall.
47. Susmel L, Taylor D (2007) A novel formulation of the theory of critical distances to estimate lifetime of notched components in the medium-cycle fatigue regime. *Fatigue & Fracture of Engineering Materials & Structures*. **30**: 567-581.